A Climatology of Clouds in Marine Cold Air Outbreaks in Both Hemispheres

JENNIFER K. FLETCHER,[a] SHANNON MASON,[b] AND CHRISTIAN JAKOB

School of Earth, Atmosphere, and Environment, Monash University, Clayton, Victoria, Australia

(Manuscript received 2 November 2015, in final form 27 April 2016)

ABSTRACT

A climatology of clouds within marine cold air outbreaks, primarily using long-term satellite observations, is presented. Cloud properties between cold air outbreaks in different regions in both hemispheres are compared. In all regions marine cold air outbreak clouds tend to be low level with high cloud fraction and low-to-moderate optical thickness. Stronger cold air outbreaks have clouds that are optically thicker, but not geometrically thicker, than those in weaker cold air outbreaks. There is some evidence that clouds deepen and break up over the course of a cold air outbreak event. The top-of-the-atmosphere longwave cloud radiative effect in cold air outbreaks is small because the clouds have low tops. However, their surface longwave cloud radiative effect is considerably larger. The rarity of cold air outbreaks in summer limits their shortwave cloud radiative effect. They do not contribute substantially to global shortwave cloud radiative effect and are, therefore, unlikely to be a major source of shortwave cloud radiative effect errors in climate models.

1. Introduction

The importance of cloud feedbacks on climate sensitivity and its uncertainty are well established (Schneider 1972; Wetherald and Manabe 1988; Soden and Held 2006; Bony et al. 2015), and it is clear that tropical and subtropical clouds play a major role in these feedbacks (e.g., Bony and Dufresne 2005). It has been argued that extratropical clouds also play an important role in climate sensitivity through feedbacks on storm strength and frequency changes (Tselioudis and Rossow 2006), shifts in jet latitude (Grise et al. 2013), and phase changes (McCoy et al. 2014).

Extratropical clouds have been shown to be important for circulation biases in climate models. Hwang and Frierson (2013) found a relationship between shortwave cloud radiative effect errors over the Southern Ocean and the double intertropical convergence zone bias in climate models, while Ceppi et al. (2012) found that shortwave errors were associated with biases in the position of the Southern Hemisphere eddy-driven jet. Trenberth and Fasullo (2010) found a correlation between the Southern Hemisphere shortwave radiation budget and climate sensitivity, with more realistic models having higher sensitivity. Beyond the general association of extratropical clouds with climate sensitivity, many questions about the role of extratropical clouds in the climate system remain.

In this study, we focus on extratropical clouds that have not been previously studied in a climatological sense: those embedded within marine cold air outbreaks (MCAOs). Individual cold air outbreaks over mid- and high-latitude oceans have been well documented for their distinctive cloud features, including striking mesoscale organization (Atkinson and Zhang 1996; Brümmer and Pohlmann 2000, and references therein). These include cloud streets—long roll clouds typically oriented along the mean wind—as well as cellular convection. Different mesoscale shallow convective organization patterns are associated with different relative strengths of shear and convective instabilities as well as Ekman layer dynamics; see the reviews by Brown (1980), Agee (1987), and Atkinson and Zhang (1996). In individual case studies and satellite imagery of MCAOs, transitions from fog to roll convection to open cellular convection often occur (Brümmer 1999). In other cases, near the ice edge MCAOs have

Denotes Open Access content.

[a] Current affiliation: University of Leeds, Leeds, United Kingdom.
[b] Current affiliation: University of Reading, Reading, United Kingdom.

Corresponding author address: Jennifer K. Fletcher, School of Earth and Environment, University of Leeds, Leeds, West Yorkshire LS2 9JT, United Kingdom.
E-mail: jennifer.fletcher@leeds.ac.uk

DOI: 10.1175/JCLI-D-15-0783.1

been observed to feature a transition from a completely cloud-covered boundary layer to one of open cells (Field et al. 2014).

Because extratropical clouds are strongly tied to circulation, previous studies have used compositing to identify the properties of clouds associated with specific circulation features, such as cyclones and fronts (e.g., Field and Wood 2007; Naud et al. 2012, 2013). Fletcher et al. (2016, hereafter FMJ16) developed a method for compositing marine cold air outbreaks. They used this method to compare the synoptic-scale flow and boundary layer structure associated with these features between the two hemispheres. We have extended this work to study the climatology of clouds and radiation associated with MCAOs and examine how that climatology depends on hemisphere, season, and strength of MCAO.

FMJ16 found that Southern Hemisphere (SH) MCAOs were weaker and smaller in horizontal scale than their Northern Hemisphere (NH) counterparts, but both existed in similar synoptic conditions. They were found in the cold air sector of extratropical cyclones, optimally positioned for cold air advection over relatively warm seas. In the NH this generally involves advection of polar continental air, while in the SH MCAOs usually originate over sea ice. FMJ16 found that MCAOs have horizontal scales on the order of 1000 km, with more intense MCAOs being much larger than less intense ones. They were characterized by strong surface sensible heat fluxes (averaging around 200 $W m^{-2}$ in a composite, but much greater in individual cases), weak low-level vertical shear due to convective momentum transport, and boundary layer deepening from around 500 m to about 2 km over the course of the MCAO trajectory.

FMJ16 also found that MCAOs are about 70% more common in NH winter than in SH winter. Conversely, summertime MCAOs are almost nonexistent in the NH while in the SH they are rare but still occur. In the shoulder seasons (spring and autumn) MCAOs in both hemispheres occur with similar frequency: about half as often as they occur in NH winter and slightly less often than SH winter. Shoulder season MCAOs are also weaker than their wintertime counterparts in each respective hemisphere. However, MCAOs are meteorologically similar events in all seasons, with strength, rather than season, as the most important way to differentiate them. Strong events in winter are more like strong events in spring than they are like weak events in winter.

To our knowledge there has been no climatological study of cold air outbreak clouds. This paper aims to fill that gap by documenting the satellite observed characteristics of clouds within MCAOs and comparing those characteristics between hemispheres and for different strengths of MCAOs. The questions we address include the following:

- How do the properties of clouds—fractional area, optical thickness, cloud-top height, phase, and radiative effect—differ from the average properties of clouds over the mid- and high-latitude oceans? How do those properties depend on season, hemisphere, region, and strength of MCAOs?
- What is the overall contribution of MCAOs to the global cloud radiative effect? Cold air outbreaks have been cited as an area of interest for model errors in clouds (e.g., Field et al. 2014).

Because our target is a long-term climatology of MCAO clouds, we primarily have used data from the International Satellite Cloud Climatology Project (ISCCP; Rossow and Schiffer 1991). We also show results from a multisensor cloud profiling dataset, described below, but we largely have left analysis of MCAO clouds with more modern but shorter-term remote sensing datasets for future work. Section 2 describes our data, our definition of MCAOs, and our compositing method; section 3 presents and discusses satellite observations of MCAO clouds; and section 4 summarizes our most important results and discusses questions we have not yet answered.

2. Method and data

a. *MCAO index*

We use the European Centre for Medium-Range Weather Forecasts (ECMWF) interim reanalysis (ERA-Interim) product (Dee et al. 2011) to define an MCAO index, as in FMJ16. We use 6-hourly instantaneous sea level pressure, 800-hPa temperature, and skin temperature for the years 1985–2009. Our index is a simple stability parameter:

$$M = \theta_{\mathrm{SKT}} - \theta_{800}, \tag{1}$$

where θ_{SKT} and θ_{800} are the potential temperatures of the surface skin and at 800 hPa, respectively. This index is similar to that developed by Kolstad and Bracegirdle (2008), and modifications on it have been used in existing studies of MCAOs, particularly those focusing on the Southern Hemisphere (Bracegirdle and Kolstad 2010; Papritz et al. 2015; FMJ16). Our MCAO index dataset is defined on a $1° \times 1°$ grid and then interpolated to the ISCCP $2.5° \times 2.5°$ grid; we excluded land areas after interpolation.

We define MCAOs as oceanic regions where $M > 0$. However, many events, especially in the Northern

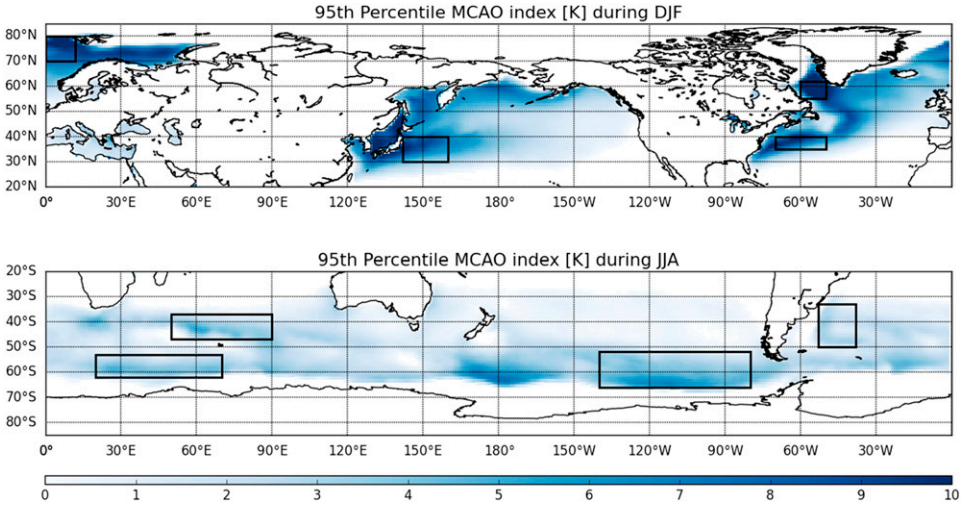

FIG. 1. Value of the 95th percentile of M (K) during winters. Black boxes show the regions used for compositing. Region names are as follows: (top) Northern Hemisphere: Norwegian Sea, Kuroshio, Gulf Stream, and Labrador Sea; (bottom) Southern Hemisphere: Indian Ocean polar front, Indian Ocean subtropical front, Bellingshausen Sea, and Brazil Current.

Hemisphere, have much larger values of M. The climatology of wintertime extremes in M is shown in Fig. 1, which highlights areas of strong MCAOs used in our analysis below. As discussed by FMJ16, MCAOs are stronger in the NH than in the SH. We divided the annual MCAO data into terciles of strength, with different tercile boundaries for each hemisphere. These tercile boundaries are provided in Table 1. Mean cloud properties were computed within each tercile as well as for all MCAOs.

Except where stated otherwise, we use data for all seasons. Because MCAOs are much more frequent in winter than other seasons (FMJ16), that season tends to dominate the statistics. However, shoulder seasons provide more opportunities for satellite observations requiring daylight. Including these seasons is necessary for robust statistics. Summertime MCAOs are uncommon and have little effect on annual mean statistics.

b. Cloud data

1) ISCCP FD

We use the ISCCP-FD product (Zhang et al. 2004) to characterize the mean cloud and radiation features of MCAOs. ISCCP-FD provides global long-term cloud and radiation observations every 3 h over a 2.5° × 2.5° grid. The MCAO index data was interpolated to this grid prior to analysis. We used the subset of ISCCP-FD from 1985 to 2009 and subsampled at the 6-hourly times corresponding to our MCAO index dataset. ISCCP-FD fields used are optical thickness, cloud fraction, and both surface and top-of-the-atmosphere (TOA) clear-sky and all-sky radiative fluxes. We used the latter to compute shortwave and longwave cloud radiative effect (SWCRE and LWCRE, respectively) at the TOA and surface. Optical thickness and shortwave fluxes were only available during the day.

2) ISCCP D1

To analyze the range of cloud types within MCAOs, we use the ISCCP-D1 cloud-top pressure-optical thickness (CTP-τ) histograms (Rossow and Schiffer 1999). In this dataset, each pixel in a 280 × 280 km^2 box is assigned to a cloud-top pressure and optical thickness bin. The resulting product gives histograms of cloud fraction by cloud top and optical thickness within each box. The temporal frequency of ISCCP-D1 is identical to that of ISCCP-FD; we used 6-hourly data from 1985 to 2009 for latitudes 30°–60°N/S.

3) DARDAR

We examined vertical profiles of cloud fraction and phase using the raDAR-liDAR (DARDAR) v2 data product, produced by Delanoë and Hogan (2010) and modified by Ceccaldi et al. (2013). DARDAR provides collocated measurements from three A-Train satellites: the Cloud Profiling Radar on *CloudSat*, the lidar and infrared radiometer on board *Cloud–Aerosol Lidar and*

TABLE 1. Values of M within terciles for each hemisphere.

	Tercile 1	Tercile 2	Tercile 3
NH	0–1.5 K	1.5–3.3 K	>3.3 K
SH	0–0.8 K	0.8–2.0 K	>2.0 K

Infrared Pathfinder Satellite Observations (*CALIPSO*), and the Moderate Resolution Imaging Spectroradiometer (MODIS).

The DARDAR algorithm uses these measurements to produce a high-resolution (60-m vertical, 1-km horizontal) estimate of cloud phase and ice water content. The phase classification also uses the ECMWF analysis wet-bulb temperature to diagnose ice or liquid for temperatures below −40°C or above 0°C, respectively. Cloud layers greater than 300 m thick with wet-bulb temperatures below zero are automatically classified as ice. Comparisons of DARDAR phase classifications with those of airborne radar/lidar found that, in individual instances, this geometric thickness threshold led to an underestimation of supercooled liquid water and overestimation of ice (Ceccaldi et al. 2013).

We used DARDAR for two winters during 2008–09: January–February in the Northern Hemisphere and July–August in the Southern Hemisphere. Substantial spans of data are missing during December and June for this 2-yr period; this is why we excluded these months.

c. Cloud radiative kernels

Zelinka et al. (2012) developed a set of so-called cloud radiative kernels to calculate the radiative impact of different clouds within the CTP-τ space of the ISCCP D1 histograms. These kernels give the change in TOA radiative fluxes per change in cloud fraction within each CTP-τ bin for average conditions. They calculated the kernels we use by applying a radiative transfer model to ERA-Interim monthly, zonal mean profiles of temperature and humidity. (These kernels are currently available online at https://markdzelinka.wordpress.com/kernels/.) We use these kernels to examine the radiative impacts of different cloud types within MCAOs, and to determine which cloud types account for the radiative differences between MCAOs. Because cold air outbreaks by definition involve very different temperature profiles than those used in the kernel calculations, we only show results for shortwave radiation.

d. Compositing

In addition to calculating the cloud properties of MCAOs on a local, gridpoint-by-gridpoint basis, we wish to characterize the cloud features of MCAOs in their meteorological context. We achieve this by compositing observed cloud properties over MCAO events. Our method of compositing is identical to that of FMJ16 and is described in detail there. To briefly summarize: we first identified regions of high MCAO activity. These regions are shown in Fig. 1. Figure 1 shows wintertime MCAOs only; however, the locations of high MCAO activity are similar in shoulder seasons. Within each region we identified MCAO events as continuous areas of $M > 0$, and we characterized the strength of each event by $M_{\max}$, the maximum value of M within the enclosed area. We centered our composites on the location of $M_{\max}$ and performed separate composites for different strength categories. We used the same strength categories as FMJ16, but we only show composites for events with $M_{\max} > 6$ K (strong events).

Additionally, we required all MCAOs included in the composite to have length scales within 50% of the mean for their strength category. We define their length scales as their longest contiguous distance both zonally and meridionally. This ensures that we composite events of similar size and orientation.

We interpolated all events from ISCCP's 2.5° × 2.5° grid to a 4000 × 2000 km^2 grid, with 200-km spacing, prior to compositing.

3. Results

a. Mean cloud properties

1) Hemispheric means and annual cycle

Figure 2 shows the area-weighted annual mean cloud properties of MCAOs in the Northern and Southern Hemisphere midlatitudes. Here "MCAO" refers to any oceanic grid point with $M > 0$, as opposed to the event composites discussed below. The MCAO grid points are differentiated by strength into the first and third terciles for each hemisphere as discussed in section 2a. Also shown are the average cloud properties for all oceanic points 30°–60°N/S during this period. All oceanic areas show high cloud fraction, consistent with the large "background" cloud field discussed by Tselioudis et al. (2000). MCAOs have somewhat higher cloud fraction than average (except weak SH cases), but they have lower optical thickness, shortwave cloud radiative effect (normalized by insolation), and TOA longwave cloud radiative effect than the oceanic average. However, the surface longwave cloud radiative effect is considerably higher in cold air outbreaks especially strong cold air outbreaks than average. The warming effect of the clouds on the surface partially offsets the strong surface cooling from turbulent heat fluxes. This is discussed more in section 3e.

Cloud fraction values around 0.7–0.9, along with slightly lower-than-average optical thickness and weak TOA LWCRE, are consistent with what we might broadly expect from MCAOs based on case studies (see e.g., Atkinson and Zhang 1996): low-level, somewhat broken stratiform clouds.

Strong MCAOs are cloudier than weak MCAOs in both hemispheres. They have greater cloud fraction and optical thickness, resulting in greater normalized

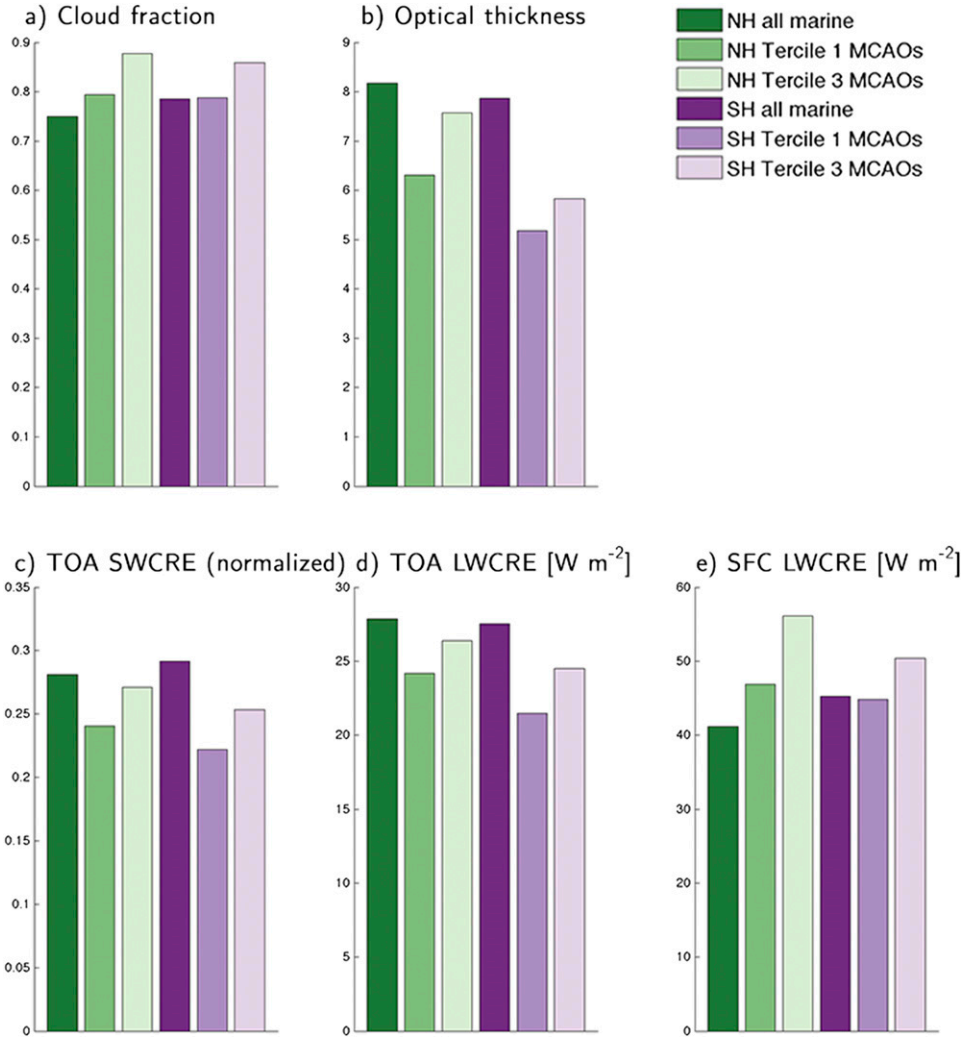

FIG. 2. ISCCP FD mean properties, 30°N/S–60°N/S: (a) cloud fraction, (b) optical thickness, (c) top-of-the-atmosphere shortwave cloud radiative effect (normalized by insolation and multiplied by −1.0), (d) top-of-the-atmosphere longwave cloud radiative effect (W m^{-2}), (e) surface longwave cloud radiative effect (W m^{-2}).

shortwave cloud radiative effect, and they might have higher cloud tops as evidenced by the increased longwave TOA cloud radiative effect (this is confirmed in section 3d).

Figure 3 shows the annual cycle in MCAO clouds from ISCCP FD. Northern Hemisphere tercile 3 MCAOs have comparatively low cloud fraction and optical thickness and consequently weak cloud radiative effect. These events are rare, with each month containing about 100 data points for all locations and all 25 years of data. Further analysis (not shown) showed that about one-third of these come from the Black, Caspian, and Aral Seas of eastern Europe and west Asia. Strong summertime cold air outbreaks over these inland seas produce fewer and optically thinner clouds than most other cold air outbreaks. In other seasons and terciles the impact of these seas is negligible, but in this case they bring down the average noticeably, with, for example, average July–August cloud fraction of 0.59 as opposed to 0.68 as seen in strong summertime MCAOs over the Atlantic. Comparing Figs. 2a and 3a shows that the drop in summertime cloudiness has almost no effect on the annual mean due to the vanishingly small number of summertime events. This dramatic drop in cloudiness is not seen in weak NH summertime MCAOs.

The other major seasonal signal is in the SWCRE, where the annual cycle in insolation determines the overall magnitude of SWCRE. This is why, for the remainder of the paper, we show SWCRE results normalized by insolation.

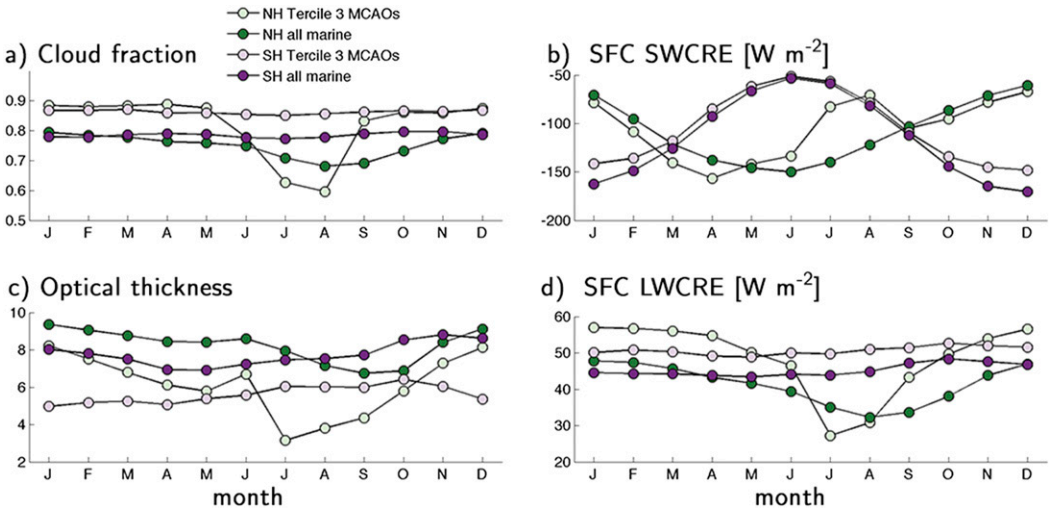

FIG. 3. (a)–(d) Annual cycle of ISCCP FD properties in all marine grid points (dark colors) and MCAOs (light colors) in both hemispheres. Data are for 30°N/S–60°N/S. Surface SWCRE and LWCRE in (b) and (d) are in W m^{-2}.

Apart from SWCRE and the NH summertime drop in strong MCAO clouds, Fig. 3 shows that there is a greater difference between category (MCAOs vs all marine grid points) than there is between seasons within a category. MCAOs almost always have greater cloud fraction, lower optical thickness, and greater surface LWCRE than marine grid points generally, regardless of season. This justifies our use of all seasons in most of the results presented below.

2) REGIONAL COMPOSITES

Whereas Figs. 2 and 3 show MCAO cloud properties averaged on a gridpoint-by-gridpoint basis, Figs. 4 and 5 show composites of clouds in strong MCAOs for selected regions of strong MCAO activity in the Northern and Southern Hemispheres, respectively. The regions, a subset of those used by FMJ16, are indicated in Fig. 1. We exclude a few of the regions from FMJ16 in the interest of space; their results are already represented by other regions that we do show. Sea level pressure contours are overlaid for reference. The dotted lines show the average location of the $M = 0$ contour (i.e., the average edge of the MCAO events composited). For reference, we also show the distribution of MCAO event strength (the value of $M_{\max}$ within the MCAO event) for each region.

In most panels in Figs. 4 and 5, the regions of highest cloud fraction appear in the locations one would expect to see fronts. Areas of lowest cloud fraction are associated with land—to the northwest in the NH panels (the signature of Cape Farewell on the tip of Greenland also appears in the northeast quadrant of Fig. 4d) and in the Brazil Current region in the SH. Previous researchers (e.g., Rossow and Schiffer 1999) have found that ISCCP measures considerably lower cloud fraction over land than over ocean.

Figures 4e–h and 5e–h show optical thickness, which in MCAOs is low to moderate (5–20) in general. In the NH, areas of locally high optical thickness are associated with warm fronts outside of the MCAO itself (or ice in the case of the Labrador and Norwegian Seas), while in the SH high optical thickness tends to occur upstream of the MCAO in the vicinity of the postfrontal ridge.

In the NH (Fig. 4), the Kuroshio and Gulf Stream composites represent regions where MCAOs occur because cold continental air is advected over warm western boundary current waters. FMJ16 found that these regions produce the most intense and frequent MCAOs. These regions, especially the Gulf Stream, contribute most to NH MCAOs having optically thicker clouds with slightly higher cloud fraction than SH MCAOs in Figs. 2a,b. Outside of western boundary current regions (e.g., the Norwegian and Labrador Seas), cloud fraction and optical thickness are generally lower in the NH MCAOs than in the SH.

Figures 4f–p and 5f–p show the surface SWCRE and LWCRE in the composites. SWCRE has been normalized by insolation. We show only the surface cloud radiative effects because Fig. 2 showed that surface LWCRE was about twice the TOA values, and because surface and TOA SWCRE are similar.

Regions of high cloud fraction or optical thickness are associated with high absolute SWCRE within the composites. The exception to this is regions with high sea ice cover (e.g., to the northwest in the Labrador Sea panels in Fig. 4), where the underlying surface albedo is high

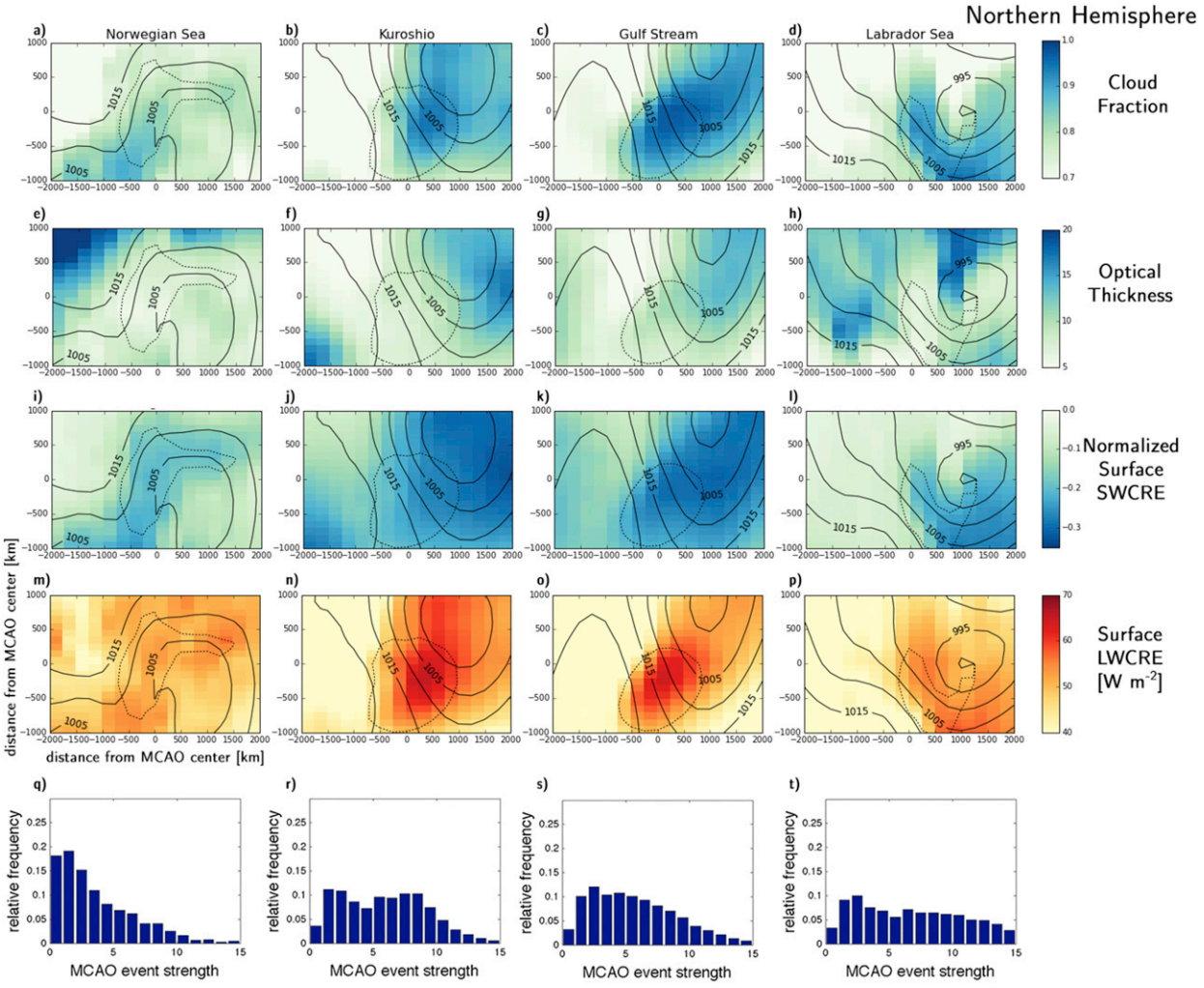

FIG. 4. (a)–(p) ISCCP FD composites for MCAO events with $M_{max} > 6$ K in four NH regions. Composite centered on the location of M_{max} within each event. Composite sea level pressure contours are overlaid for reference. Dashed lines show mean location of $M = 0$ contour (MCAO boundary). (q)–(t) Distribution of value of M_{max} in each region.

and SWCRE is therefore low. In all regions except the high-latitude NH, there is substantial SWCRE not only within the MCAO but in the entire equatorward section of the associated surface low. In the SH, high SWCRE also occurs in the postfrontal ridge. The reason this is so much cloudier in the Southern than the Northern Hemisphere is likely because NH MCAOs usually originate over land, which would be to the west in these plots, while SH MCAOs originate over sea ice.

The LWCRE in Figs. 4 and 5 appears closely tied to the cloud fraction in all regions. Any area with cloud fraction over about 0.9 has surface LWCRE of at least 50–60 W m^{-2}. This mostly occurs within the MCAOs and near the associated low. This LWCRE warms the surface and mostly offsets the wintertime SWCRE, which ranges from 50 to 100 W m^{-2}.

It is possible that the reduction in cloud fraction and optical thickness downstream of the MCAO maximum represents a transition from closely spaced rolls or stratiform cloud cover/fog to open cellular convection. Testing this hypothesis will be included in future work on mesoscale convective organization in MCAOs.

b. *Cloud types in MCAOs*

ISCCP FD provides the bulk properties within a grid cell, while ISCCP D1 describes the range of cloud types within the cell via histograms of cloud fraction binned by optical thickness (τ) and cloud-top pressure. Figures 6a,b and 6e,f show the mean ISCCP histograms for all maritime midlatitude (30°–60°N/S) grid points and for all MCAOs. Figures 6c,d and 6g,h also show how clouds within the strongest and weakest terciles of MCAO

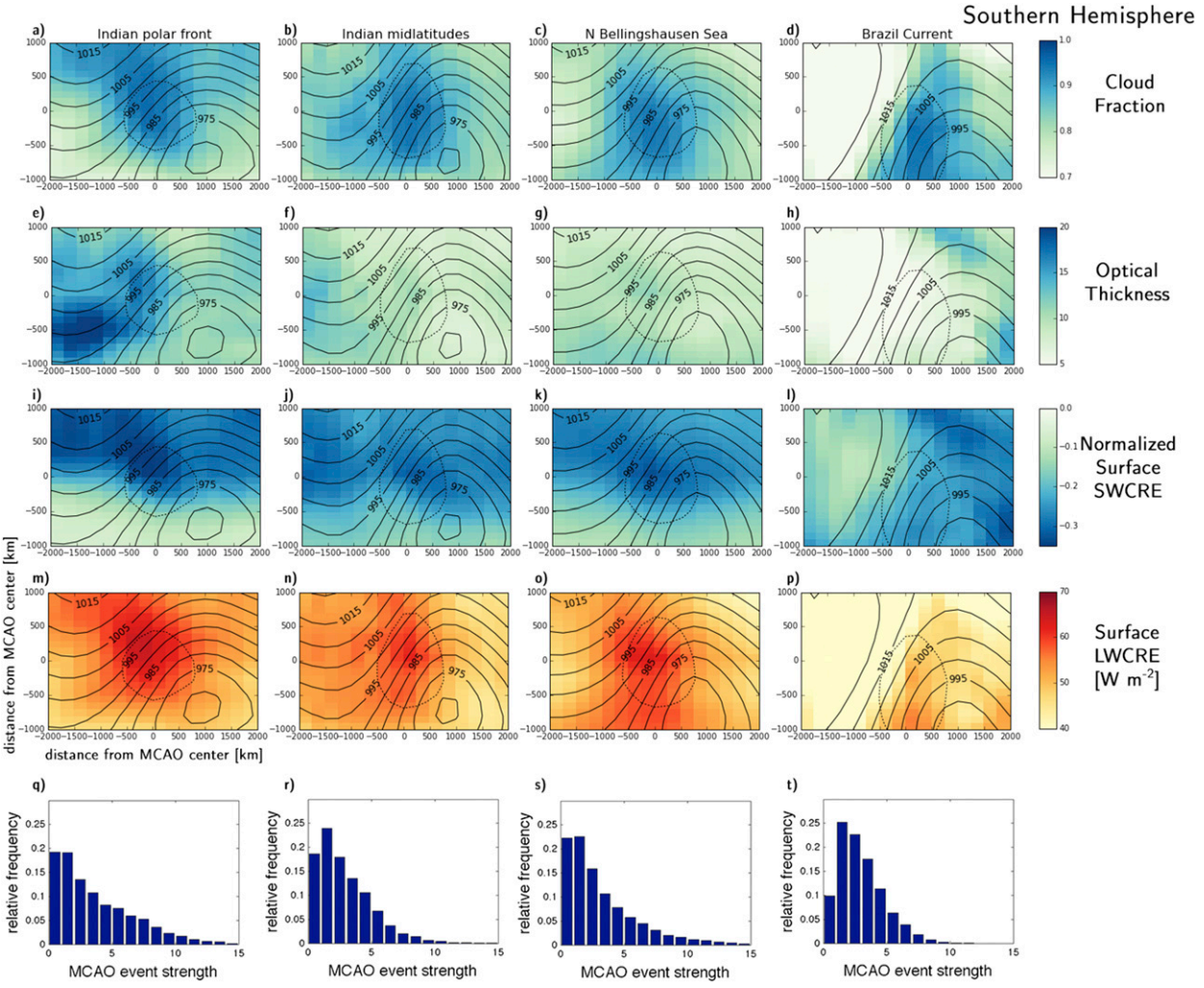

FIG. 5. (a)–(p) ISCCP FD composites for MCAO events with $M_{max} > 6$ K in four SH regions. Composite centered on the location of M_{max} within each event. Composite sea level pressure contours are overlaid for reference. Dashed lines show mean location of $M = 0$ contour (MCAO boundary). (q)–(t) Distribution of value of M_{max} in each region.

strength differ from the MCAO mean. Results are for all seasons.

The histograms are consistent with other results: MCAOs have higher cloud fraction but tend to occupy lower optical thickness bins than average. This is most noticeable in the bins of mid- to high cloud tops and mid- to high optical thickness. These higher-topped clouds account for the greater optical thickness in the midlatitude marine average than in MCAOs shown in Fig. 2b. In both hemispheres the upper tercile MCAOs have considerably higher optical thickness than the lower tercile MCAOs. In the Northern Hemisphere the clouds in strong MCAOs have slightly lower tops than those in weak MCAOs. In the Southern Hemisphere most of the clouds are low level but most of the difference between terciles comes from midlevel clouds, with the strongest MCAOs having more optically thick midlevel clouds than average. ISCCP is known to misclassify some optically thin high cloud over low cloud scenes as midlevel (Jin and Rossow 1997; Marchand et al. 2010). We explore this more in Sections 3c and 3d.

Figure 6 also shows the shortwave impacts of the cloud anomalies within MCAOs. To calculate this we used the radiative kernels of Zelinka et al. (2012) discussed in section 2c. The kernels give the change in TOA fluxes due to changes in cloud fraction within each CTP-τ bin. We multiply these kernels by the ISCCP D1 cloud fraction anomalies associated with MCAOs shown in Figs. 6a–h. The first two columns show the annual mean shortwave cloud radiative effect for each ISCCP bin for all midlatitude oceanic points and for MCAOs, respectively. The optically thicker clouds in

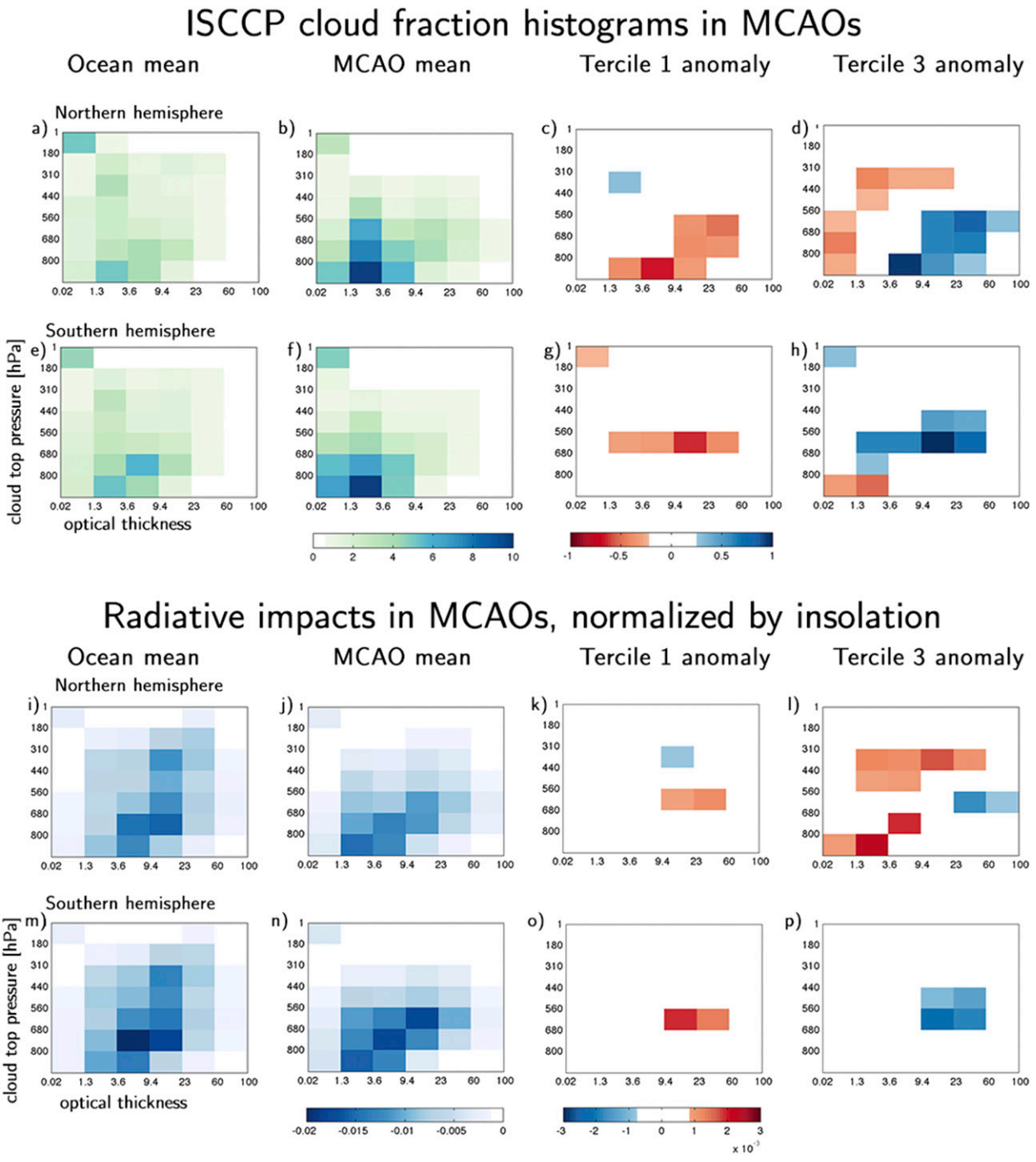

FIG. 6. (a),(b),(e),(f) ISCCP D1 joint CTP-τ histograms of cloud fraction for all oceanic extratropics, all MCAOs. (c),(d),(g),(h) First and third strength tercile cloud fraction anomaly from the MCAO mean. (i)–(p) As in (a)–(h), but for the TOA SWCRE ($W\,m^{-2}$) associated with the corresponding cloud fraction histograms. Note that blue colors indicate more clouds or stronger (absolute) SWCRE in all panels.

τ bins between 3.6 and 23 produced a disproportionate amount of the shortwave cloud radiative effect associated with MCAOs even though they occur less frequently than lower τ clouds. This follows from the relationship between SWCRE and optical thickness (Nakajima and King 1990).

Figures 6j,k and 6m,n show the anomalous radiation associated with the weakest and strongest terciles

of MCAOs. In both hemispheres the stronger and more optically thick tercile unsurprisingly is associated with greater shortwave cloud radiative effect. The strongest NH MCAOs have fewer mid- to high-topped clouds of moderate optical thickness, which partially offsets the increase in low- to midtopped optically thick clouds.

c. Cloud regimes found in MCAOs

Tselioudis et al. (2013) used k-means clustering to sort ISCCP-D1 histograms into 12 regimes, which they call "weather states" and that may be associated with well-known cloud morphologies or environments. We show the distribution of these cloud regimes for maritime midlatitudes and for MCAOs in Figs. 7a–f. Because the MCAO cloud regimes are similar for all types of MCAOs, we display the tercile results in terms of their difference from the oceanic mean rather than from the MCAO mean. For reader convenience, Figs. 7g–q shows the ISCCP CTP-τ histograms associated with each regime from Tselioudis et al. (2013). Regime 12, clear sky, is omitted.

Compared to the maritime average, MCAOs have high representation of the following regimes: regime 5, a midlevel regime with low-to-moderate optical thickness; and regime 8, which Tselioudis et al. (2013) call "shallow cumulus." Regime 8 is by far the most common. We speculate that this regime is identified within MCAOs during instances of open cellular convection.

Conversely, MCAOs have the following regimes underrepresented compared to the maritime average: regime 1, associated with deep convection; regime 2, associated with fronts; regime 3, associated with stratiform anvils; regime 7, which Tselioudis et al. (2013) call "fair weather," associated with a range of clouds and low overall cloud fraction; and regime 12, clear sky. Additionally, MCAOs in the Southern Hemisphere have fewer occurrences of regimes 9–10, stratocumulus clouds of moderate optical thickness. The SH MCAOs instead are observed more frequently with regime 5, midtopped clouds of lower optical thickness than regime 9. However, Mason et al. (2014) found that a similar ISCCP cloud regime (called M1 in their paper) was classified by DARDAR as having only low clouds about 40% of the time and both low- and midlevel clouds about 30% of the time. Regime 5 does contain low cloud, but the ratio of midlevel to low cloud is greater than what likely occurs in SH MCAOs (as demonstrated in the next section). Some instances of regime 5 are likely low cloud and may include the shallow or open cellular convection associated with regime 8.

There is little difference between first and third tercile MCAO clouds within each hemisphere. Both show a slight increase in regime 4 and a decrease in regime 7 for stronger MCAOs, consistent with Fig. 6 showing tercile differences primarily in midtopped clouds of moderate- to high optical thickness. As above, this may reflect the ISCCP D1 dataset's midlevel bias.

d. Cloud profiles

We examined profiles of cloud phase within MCAOs derived in the DARDAR dataset. Here we identified continuous areas with all grid points having M greater than a threshold and averaged DARDAR quantities for any passes that occur over such areas within 1 hour. Table 2 shows the number of MCAO areas for each hemisphere and M threshold used; these areas are of MCAO scales and several hundred to several thousand DARDAR profiles each.

Figure 8 shows that DARDAR predominantly assigns clouds in MCAOs to the ice phase. Mixed phase (labeled ice + SLW) and supercooled liquid water (SLW) are the second and third most-frequently diagnosed, but are much less common. DARDAR has additional rain and warm cloud categories, but those are rarely seen in MCAOs and are not shown here. DARDAR finds considerably more cloud within stronger MCAOs, with most of the difference coming from the ice phase. Weak SH MCAOs have the greatest supercooled liquid water of any categories shown. Figure 8d shows the SLW fraction, SLW/(SLW + ice + mixedphase). MCAOs have SLW fraction around 0.05–0.1 in the lowest 2 km, lower than the maritime average of 0.05–0.5.

Figure 8 also shows that most MCAOs have cloud tops around 2 km. This is consistent with the ISCCP results in Fig. 6, which show that most cloud-top pressures are greater than 680 hPa, especially in the SH. Furthermore, cloud fraction drops off more rapidly with height in strong MCAOs than in weak ones or (much more markedly) in the maritime average. This is consistent with the lower cloud tops seen in strong MCAOs by ISCCP in Fig. 6 for the NH, but ISCCP does not show this in the SH (if anything, the ISCCP results suggest higher cloud tops in strong SH MCAOs compared to weak ones). However, the difference shown in cloud top in the DARDAR results is smaller than the difference in cloud fraction at around 1.5 km. ISCCP does not pick up this difference, possibly because it is masked by cloud above 1.5 km.

Because of surface clutter in the radar and attenuation of lidar in liquid and mixed-phase cloud, DARDAR cloud fraction is underestimated in the lowest 1 km of the profile (Protat et al. 2014). There is therefore a high level of uncertainty in cloud base. Nonetheless, the difference in cloud tops as seen by DARDAR strongly suggests that clouds within MCAOs are geometrically

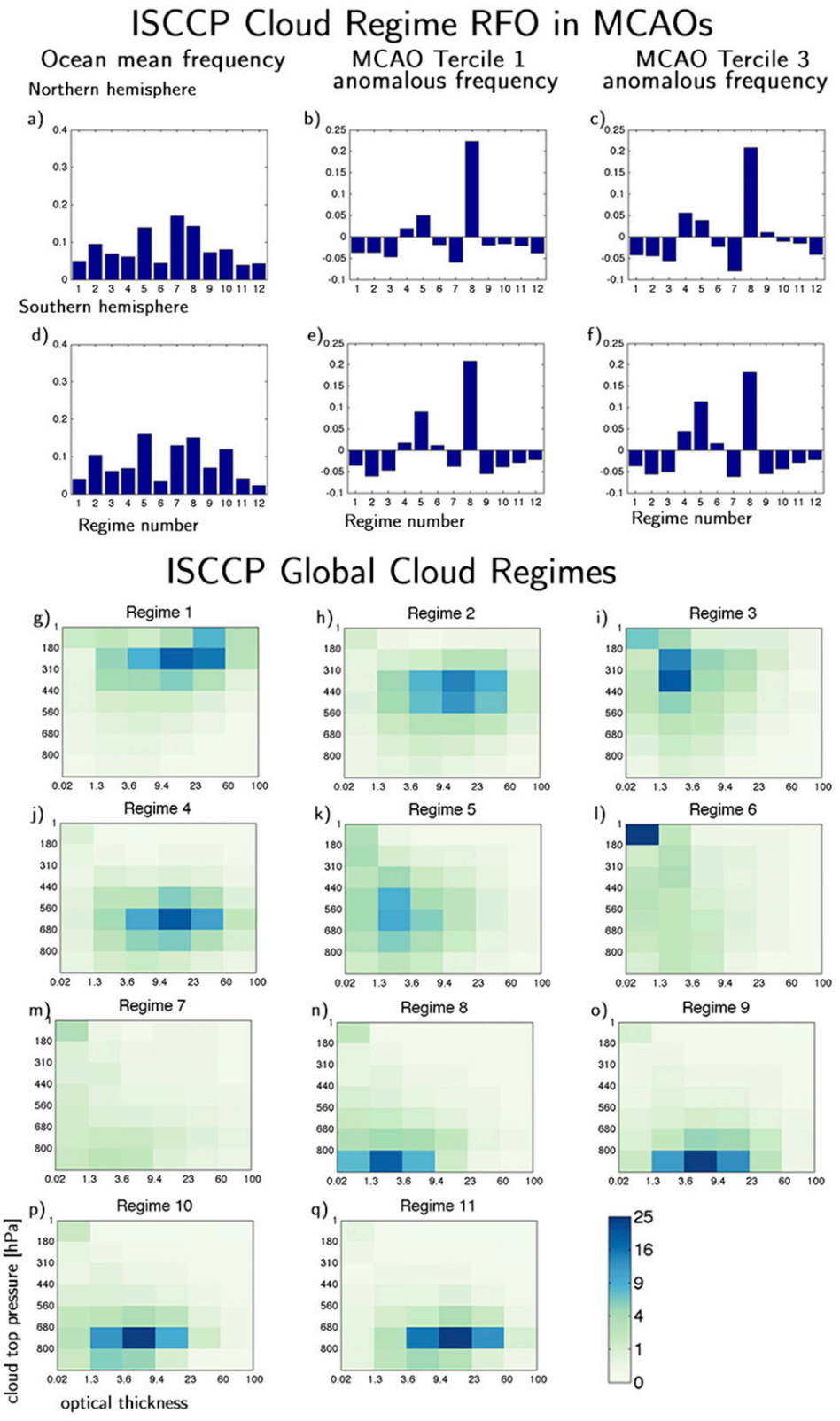

FIG. 7. (a),(d) Frequency of occurrence of global cloud regimes for all NH and SH midlatitude marine gridpoints. (b),(c),(e),(f) Anomalous frequency of occurrence of global cloud regimes for MCAO terciles 1 and 3 from the oceanic mean. (g)–(q) ISCCP global cloud regimes from Tselioudis et al. (2013).

TABLE 2. Number of MCAO events in DARDAR data.

	$M > 0$	$M > 5$
NH	242	15
SH	184	14

thinner than the maritime average. The average cloud fraction within MCAOs is around 0.05 at 5-km height, while in the maritime average it is 0.2. This may be why MCAO clouds are optically thinner than average in Fig. 2.

Figure 9 shows that strong MCAOs have much greater ice water content (IWC) than weaker MCAOs or than the marine average. This higher IWC is likely why strong MCAOs have greater optical thickness than weak MCAOs. Figure 9 also provides further evidence that strong MCAOs have lower tops than weak MCAOs in both hemispheres.

There has recently been a lot of attention given to the high presence of SLW in clouds over the Southern Ocean. Our results suggest that, within MCAOs, SLW is fairly rare. For typical conditions over the high-latitude Southern Ocean (SST roughly 1°–5°C, sea level pressure 980–1015 hPa), $M = 6$ K corresponds to 800-hPa temperatures roughly between −23° and −16°C. Thus, one

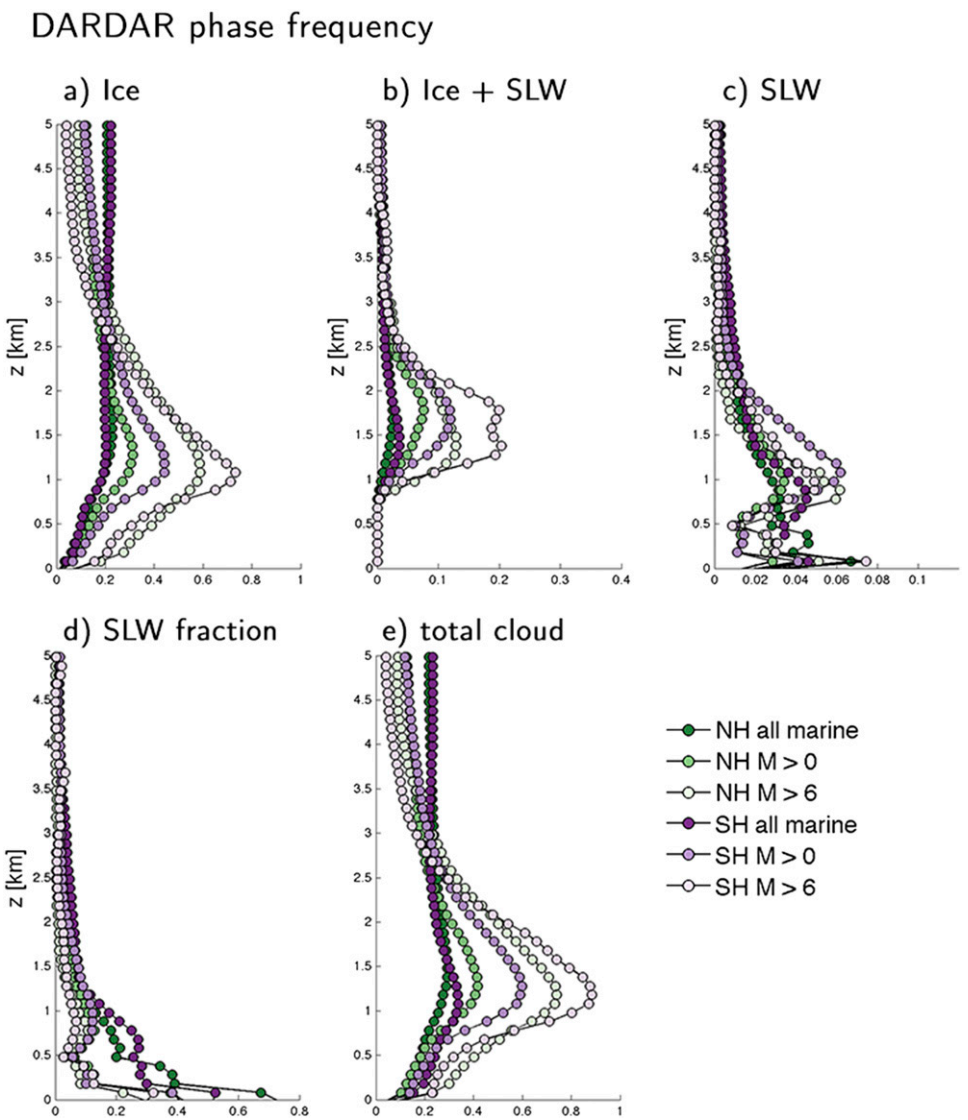

FIG. 8. (a)–(e) Relative frequency of occurrence of cloud phase in oceanic extratropics as classified by DARDAR. In (e) the sum of all phases are shown, including warm cloud and rain, which are not shown. Note that different horizontal scales are used in different panels, and that "Ice + SLW" refers to mixed phase, not the sum of ice and SLW.

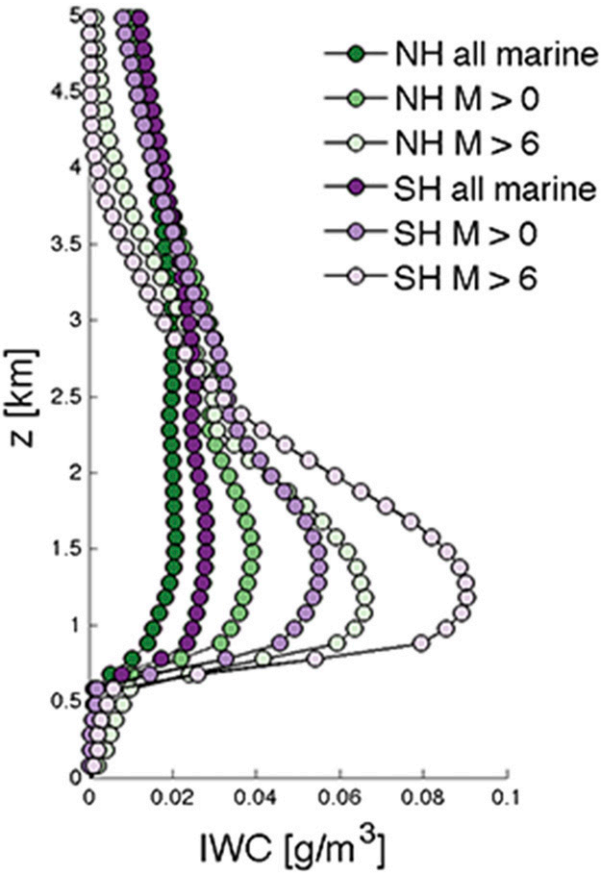

FIG. 9. Ice water content as classified by DARDAR.

would expect that supercooled liquid water might be more prevalent, especially given that Chubb et al. (2013) observed it in situ over the Southern Ocean at temperatures as low as −22°C. Huang et al. (2012) found in case studies that the DARDAR v1 algorithm often classified cloud tops as ice when *CALIPSO* classification suggested liquid or unknown, and DARDAR v2 appears to classify more scenes as ice and fewer scenes as SLW compared to v1 (Ceccaldi et al. 2013). While this shift from v1 to v2 may be more accurate overall, it has not been validated over the Southern Ocean. DARDAR's supercooled liquid water and mixed phase fractions should be regarded as a low estimate, and ice fraction should be regarded conversely as a high estimate.

e. The maximum radiative impact of MCAOs

Returning to the question of the radiative impact of clouds within MCAOs, we calculated the maximum cloud radiative effect (CRE) that could be attributed to MCAO clouds. To do this, we calculated the mean ISCCP FD surface shortwave and longwave CRE over all times, but first set CRE equal to zero for all points not within MCAOs. We then divided by the total mean CRE. This calculation represents the fractional contribution of MCAO clouds to the total cloud radiative effect. This was done separately for shortwave, longwave, and net surface CRE. This indicates the maximum model bias in CRE that could be attributed to incorrect simulation of clouds within MCAOs.

Figure 10 shows this contribution for December–February and June–August. Contours of MCAO relative frequency of occurrence are overlaid for reference. The radiative impact of MCAOs is limited by their frequency of occurrence and seasonality, especially in the SH. In the SH, the SWCRE attributable to MCAOs (Figs. 10a and 10c) is always less than 30% of the total, and is usually less than 10%. Their contribution to the longwave effect is slightly greater, around 15%–20% in winter. In the NH, MCAOs contribute a substantial fraction of the wintertime SWCRE and LWCRE. It should be kept in mind that overall SWCRE in winter is small, although among regions of high MCAO activity it is greatest in the Gulf Stream and Kurioshio, where the fractional contribution from MCAOs is also the greatest. MCAOs' contribution to the global radiation budget, therefore, lies primarily in the NH storm tracks. In the Southern Ocean region, where MCAOs have been highlighted as a possible source of model bias in clouds and radiation (e.g., Field et al. 2014), their radiative contribution is very small.

Figure 10e shows the annual mean net CRE attributable to MCAOs (this time in $\mathrm{W\,m^{-2}}$). The shortwave cooling effect dominates at lower latitudes where insolation is higher, but at higher latitudes MCAOs have a net radiative warming impact on the surface. This warming is more than offset by the substantial cooling effect of surface sensible and latent heat fluxes, which typically range from 50 to 200 $\mathrm{W\,m^{-2}}$ in MCAOs (FMJ16).

4. Conclusions

We present a climatology of clouds within MCAOs, primarily using the long-term ISCCP dataset to establish the role of MCAO clouds in climate over much of the satellite era. Our main results are as follows:

- Clouds within MCAOs have mostly higher cloud fraction but lower optical thickness, shortwave cloud radiative effect, and TOA longwave cloud radiative effect than clouds in maritime midlatitudes on average. However, they have greater-than-average surface LWCRE, especially in high latitudes, where the surface LWCRE more than offsets surface SWCRE and partially compensates for cooling by sensible heat fluxes. However, this longwave warming effect is much weaker than the anomalous surface sensible

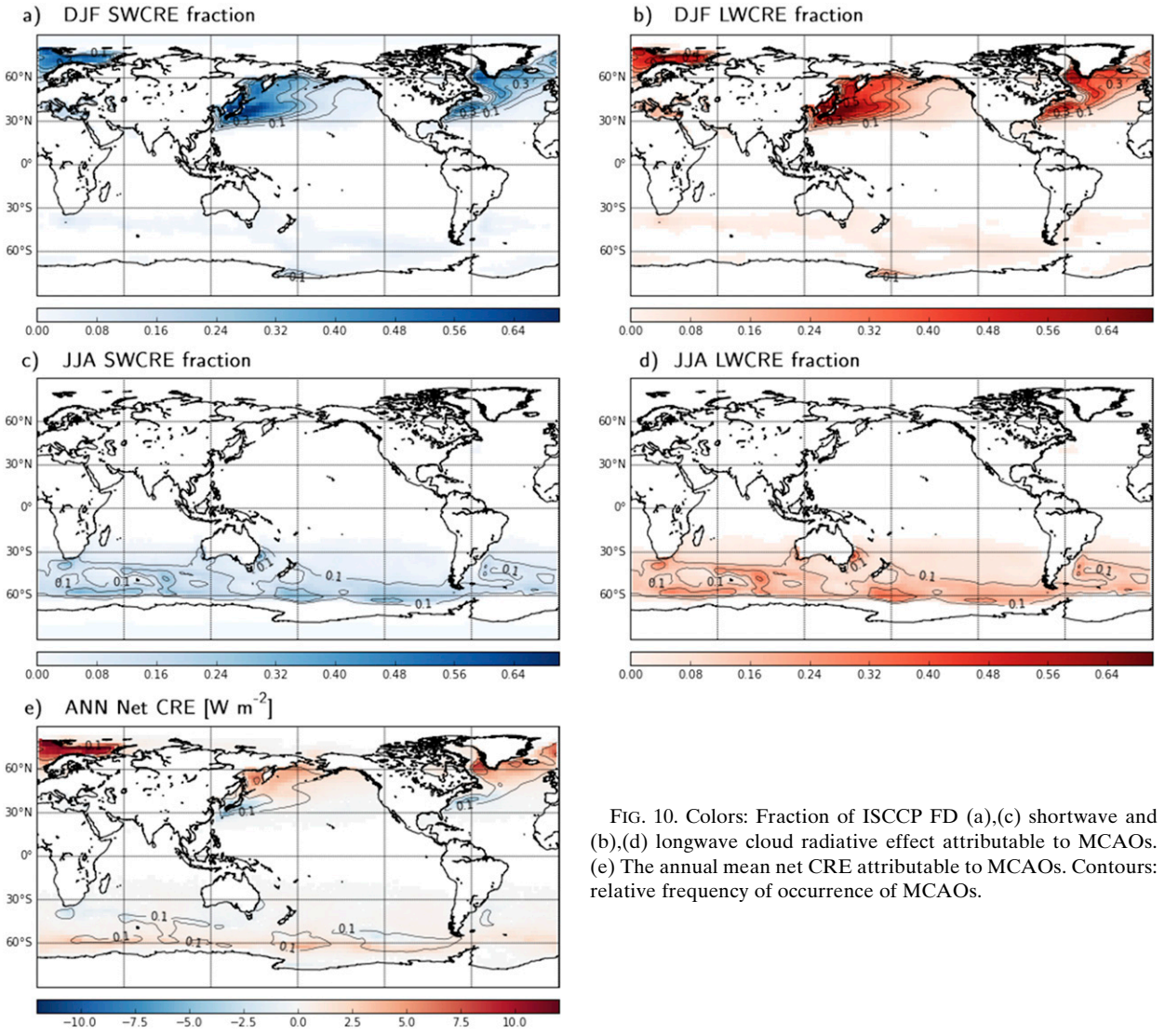

FIG. 10. Colors: Fraction of ISCCP FD (a),(c) shortwave and (b),(d) longwave cloud radiative effect attributable to MCAOs. (e) The annual mean net CRE attributable to MCAOs. Contours: relative frequency of occurrence of MCAOs.

heat fluxes, which cool the surface on the order of 100 W m^{-2} greater than usual (FMJ16), while the LWCRE warms the surface on the order of 10 W m^{-2} above average. Geometrical thinness may be responsible for the low optical thickness of MCAO clouds.

- Strong MCAOs have greater cloud fraction and optical thickness than weak MCAOs. These results hold for both hemispheres. For both hemispheres, there is a systematic shift toward higher optical thickness for stronger MCAOs. Cloud-top height varies much less, with most MCAO clouds having cloud-top pressure greater than 680 hPa and well below 2 km. However, strong MCAOs do have somewhat lower cloud tops than weak MCAOs.
- The top-of-the-atmosphere radiative impact of MCAOs is limited by two factors: their low cloud tops, which limits their TOA longwave cloud radiative effect; and their low frequency of occurrence in the warm seasons, which limits their shortwave cloud radiative effect. Their greatest radiative impact is at the surface, where the longwave effect is large enough to fully offset the surface SWCRE in winter. Additionally, NH MCAOs associated with western boundary currents may contribute substantially to overall shortwave cloud radiative effect in the midlatitudes. This is because they make up the majority of the shortwave cloud radiative effect in winter in those locations and occur at low enough latitudes that insolation is substantial even in the colder seasons. If an important cloud radiative feedback associated with cold air outbreaks does exist, it would be located in these regions rather than in the Southern Hemisphere. The simple method we use to evaluate the fractional contribution of MCAOs to CRE can be easily replicated for other types of weather and circulation systems.

The difference in cloud properties for different MCAO strengths might not reflect the differences between individual weather events so much as differences between MCAOs in different stages of development. The early stage of an MCAO, when the cold air mass has just reached open water, is often the point when it would have the highest strength classification (Fig. 1 shows the highest extreme values of M near the ice and continent edges). As surface fluxes and shallow convective mixing warm and deepen the boundary layer, as shown in FMJ16, the MCAO index will be reduced. Strong MCAOs are likely overrepresented by a shallow boundary layer with low stratiform clouds. This may then transition to a deeper, more well-mixed boundary layer with a smaller MCAO index and a deeper but more broken cloud field. The cloud fraction and optical thickness observations from ISCCP and cloud profiles from DARDAR are all consistent with this transition.

A very interesting question we have not addressed is the relationship between MCAOs and mesoscale cellular convection. This link has been studied extensively in case studies, but not climatologically, and not for the Southern Hemisphere. Muhlbauer et al. (2014) found that the highest worldwide incidence of open cellular convection occurs over the Southern Ocean in austral winter and speculated that this is due to MCAOs. The transition from low, stratiform capped boundary layer to a deeper convective boundary layer discussed above may also include a transition from closed to open cellular convection. Whether MCAOs are a useful predictor of mesoscale organization of shallow convection in the extratropics is an interesting question for further study. This climatology helps set the stage for future investigations of cloud organization (using newer satellite observations with shorter records than ISCCP) within MCAOs.

Acknowledgments. This research was supported by Australian Research Council (ARC) Discovery Grant (DP130100869) and the ARC Centre of Excellence for Climate System Science (CE110001028). We thank three anonymous reviewers whose thoughtful comments sharpened our analysis and improved our presentation.

REFERENCES

Agee, E. M., 1987: Mesoscale cellular convection over the oceans. *Dyn. Atmos. Oceans*, **10**, 317–341, doi:10.1016/0377-0265(87)90023-6.

Atkinson, B., and J. Wu Zhang, 1996: Mesoscale shallow convection in the atmosphere. *Rev. Geophys.*, **34**, 403–431, doi:10.1029/96RG02623.

Bony, S., and J.-L. Dufresne, 2005: Marine boundary layer clouds at the heart of tropical cloud feedback uncertainties in climate models. *Geophys. Res. Lett.*, **32**, L20806, doi:10.1029/2005GL023851.

——, and Coauthors, 2015: Clouds, circulation and climate sensitivity. *Nat. Geosci.*, **8**, 261–268, doi:10.1038/ngeo2398.

Bracegirdle, T. J., and E. W. Kolstad, 2010: Climatology and variability of Southern Hemisphere marine cold-air outbreaks. *Tellus*, **62A**, 202–208, doi:10.1111/j.1600-0870.2009.00431.x.

Brown, R. A., 1980: Longitudinal instabilities and secondary flows in the planetary boundary layer: A review. *Rev. Geophys.*, **18**, 683–697, doi:10.1029/RG018i003p00683.

Brümmer, B., 1999: Roll and cell convection in wintertime Arctic cold-air outbreaks. *J. Atmos. Sci.*, **56**, 2613–2636, doi:10.1175/1520-0469(1999)056<2613:RACCIW>2.0.CO;2.

——, and S. Pohlmann, 2000: Wintertime roll and cell convection over Greenland and Barents Sea regions: A climatology. *J. Geophys. Res.*, **105**, 15 559–15 566, doi:10.1029/1999JD900841.

Ceccaldi, M., J. Delanoë, R. J. Hogan, N. L. Pounder, A. Protat, and J. Pelon, 2013: From *CloudSat–CALIPSO* to EarthCare: Evolution of the DARDAR cloud classification and its comparison to airborne radar–lidar observations. *J. Geophys. Res. Atmos.*, **118**, 7962–7981, doi:10.1002/jgrd.50579.

Ceppi, P., Y.-T. Hwang, D. M. Frierson, and D. L. Hartmann, 2012: Southern Hemisphere jet latitude biases in CMIP5 models linked to shortwave cloud forcing. *Geophys. Res. Lett.*, **39**, L19708, doi:10.1029/2012GL053115.

Chubb, T. H., J. B. Jensen, S. T. Siems, and M. J. Manton, 2013: In situ observations of supercooled liquid clouds over the Southern Ocean during the HIAPER pole-to-pole observation campaigns. *Geophys. Res. Lett.*, **40**, 5280–5285, doi:10.1002/grl.50986.

Dee, D. P., and Coauthors, 2011: The ERA-Interim reanalysis: Configuration and performance of the data assimilation system. *Quart. J. Roy. Meteor. Soc.*, **137**, 553–597, doi:10.1002/qj.828.

Delanoë, J., and R. J. Hogan, 2010: Combined *CloudSat–CALIPSO*–MODIS retrievals of the properties of ice clouds. *J. Geophys. Res.*, **115**, D00H29, doi:10.1029/2009JD012346.

Field, P. R., and R. Wood, 2007: Precipitation and cloud structure in midlatitude cyclones. *J. Climate*, **20**, 233–254, doi:10.1175/JCLI3998.1.

——, R. J. Cotton, K. McBeath, A. P. Lock, S. Webster, and R. P. Allan, 2014: Improving a convection-permitting model simulation of a cold air outbreak. *Quart. J. Roy. Meteor. Soc.*, **140**, 124–138, doi:10.1002/qj.2116.

Fletcher, J. K., S. L. Mason, and C. Jakob, 2016: The climatology, meteorology, and boundary layer structure of marine cold air outbreaks in both hemispheres. *J. Climate*, **29**, 1999–2014, doi:10.1175/JCLI-D-15-0268.1.

Grise, K. M., L. M. Polvani, G. Tselioudis, Y. Wu, and M. D. Zelinka, 2013: The ozone hole indirect effect: Cloud-radiative anomalies accompanying the poleward shift of the eddy-driven jet in the southern hemisphere. *Geophys. Res. Lett.*, **40**, 3688–3692, doi:10.1002/grl.50675.

Huang, Y., S. T. Siems, M. J. Manton, A. Protat, and J. Delanoë, 2012: A study on the low-altitude clouds over the Southern Ocean using the DARDAR-MASK. *J. Geophys. Res.*, **117**, D18204, doi:10.1029/2012JD017800.

Hwang, Y.-T., and D. M. Frierson, 2013: Link between the double-intertropical convergence zone problem and cloud biases over

the Southern Ocean. *Proc. Natl. Acad. Sci. USA*, **110**, 4935–4940, doi:10.1073/pnas.1213302110.

Jin, Y., and W. B. Rossow, 1997: Detection of cirrus overlapping low-level clouds. *J. Geophys. Res.*, **102**, 1727–1737, doi:10.1029/96JD02996.

Kolstad, E. W., and T. J. Bracegirdle, 2008: Marine cold-air outbreaks in the future: An assessment of IPCC AR4 model results for the Northern Hemisphere. *Climate Dyn.*, **30**, 871–885, doi:10.1007/s00382-007-0331-0.

Marchand, R., T. Ackerman, M. Smyth, and W. B. Rossow, 2010: A review of cloud top height and optical depth histograms from MISR, ISCCP, and MODIS. *J. Geophys. Res.*, **115**, D16206, doi:10.1029/2009JD013422.

Mason, S., C. Jakob, A. Protat, and J. Delanoë, 2014: Characterizing observed midtopped cloud regimes associated with Southern Ocean shortwave radiation biases. *J. Climate*, **27**, 6189–6203, doi:10.1175/JCLI-D-14-00139.1.

McCoy, D. T., D. L. Hartmann, and D. P. Grosvenor, 2014: Observed Southern Ocean cloud properties and shortwave reflection. Part II: Phase changes and low cloud feedback. *J. Climate*, **27**, 8858–8868, doi:10.1175/JCLI-D-14-00288.1.

Muhlbauer, A., I. L. McCoy, and R. Wood, 2014: Climatology of stratocumulus cloud morphologies: Microphysical properties and radiative effects. *Atmos. Chem. Phys.*, **14**, 6695–6716, doi:10.5194/acp-14-6695-2014.

Nakajima, T., and M. D. King, 1990: Determination of the optical thickness and effective particle radius of clouds from reflected solar radiation measurements. Part I: Theory. *J. Atmos. Sci.*, **47**, 1878–1893, doi:10.1175/1520-0469(1990)047<1878:DOTOTA>2.0.CO;2.

Naud, C. M., D. J. Posselt, and S. C. Van Den Heever, 2012: Observational analysis of cloud and precipitation in midlatitude cyclones: Northern versus Southern Hemisphere warm fronts. *J. Climate*, **25**, 5135–5151, doi:10.1175/JCLI-D-11-00569.1.

——, J. F. Booth, D. J. Posselt, and S. C. van den Heever, 2013: Multiple satellite observations of cloud cover in extratropical cyclones. *J. Geophys. Res. Atmos.*, **118**, 9982–9996, doi:10.1002/jgrd.50718.

Papritz, L., S. Pfahl, H. Sodemann, and H. Wernli, 2015: A climatology of cold air outbreaks and their impact on air–sea heat fluxes in the high-latitude South Pacific. *J. Climate*, **28**, 342–364, doi:10.1175/JCLI-D-14-00482.1.

Protat, A., and Coauthors, 2014: Reconciling ground-based and space-based estimates of the frequency of occurrence and radiative effect of clouds around Darwin, Australia. *J. Appl. Meteor. Climatol.*, **53**, 456–478, doi:10.1175/JAMC-D-13-072.1.

Rossow, W. B., and R. A. Schiffer, 1991: ISCCP cloud data products. *Bull. Amer. Meteor. Soc.*, **72**, 2–20, doi:10.1175/1520-0477(1991)072<0002:ICDP>2.0.CO;2.

——, and ——, 1999: Advances in understanding clouds from ISCCP. *Bull. Amer. Meteor. Soc.*, **80**, 2261–2287, doi:10.1175/1520-0477(1999)080<2261:AIUCFI>2.0.CO;2.

Schneider, S. H., 1972: Cloudiness as a global climatic feedback mechanism: The effects on the radiation balance and surface temperature of variations in cloudiness. *J. Atmos. Sci.*, **29**, 1413–1422, doi:10.1175/1520-0469(1972)029<1413:CAAGCF>2.0.CO;2.

Soden, B. J., and I. M. Held, 2006: An assessment of climate feedbacks in coupled ocean–atmosphere models. *J. Climate*, **19**, 3354–3360, doi:10.1175/JCLI3799.1.

Trenberth, K. E., and J. T. Fasullo, 2010: Simulation of present-day and twenty-first-century energy budgets of the Southern Oceans. *J. Climate*, **23**, 440–454, doi:10.1175/2009JCLI3152.1.

Tselioudis, G., and W. B. Rossow, 2006: Climate feedback implied by observed radiation and precipitation changes with midlatitude storm strength and frequency. *Geophys. Res. Lett.*, **33**, L02704, doi:10.1029/2005GL024513.

——, Y. Zhang, and W. B. Rossow, 2000: Cloud and radiation variations associated with northern midlatitude low and high sea level pressure regimes. *J. Climate*, **13**, 312–327, doi:10.1175/1520-0442(2000)013<0312:CARVAW>2.0.CO;2.

——, W. Rossow, Y. Zhang, and D. Konsta, 2013: Global weather states and their properties from passive and active satellite cloud retrievals. *J. Climate*, **26**, 7734–7746, doi:10.1175/JCLI-D-13-00024.1.

Wetherald, R., and S. Manabe, 1988: Cloud feedback processes in a general circulation model. *J. Atmos. Sci.*, **45**, 1397–1416, doi:10.1175/1520-0469(1988)045<1397:CFPIAG>2.0.CO;2.

Zelinka, M. D., S. A. Klein, and D. L. Hartmann, 2012: Computing and partitioning cloud feedbacks using cloud property histograms. Part I: Cloud radiative kernels. *J. Climate*, **25**, 3715–3735, doi:10.1175/JCLI-D-11-00248.1.

Zhang, Y., W. B. Rossow, A. A. Lacis, V. Oinas, and M. I. Mishchenko, 2004: Calculation of radiative fluxes from the surface to top of atmosphere based on ISCCP and other global data sets: Refinements of the radiative transfer model and the input data. *J. Geophys. Res.*, **109**, D19105, doi:10.1029/2003JD004457.